Topological metamagnetism: Thermodynamics and dynamics of the transition in spin ice under uniaxial compression

L. Pili,[1,2] A. Steppke,[3] M. E. Barber,[3] F. Jerzembeck,[3] C. W. Hicks,[3] P. C. Guruciaga,[4,*] D. Prabhakaran,[5]
R. Moessner,[6] A. P. Mackenzie,[3,7] S. A. Grigera,[1,2,†] and R. A. Borzi[1,2,‡]

[1]*Instituto de Física de Líquidos y Sistemas Biológicos, UNLP-CONICET, B1900BTE La Plata, Argentina*
[2]*Departamento de Física, Facultad de Ciencias Exactas, Universidad Nacional de La Plata, B1900 La Plata, Argentina*
[3]*Max Planck Institute for Chemical Physics of Solids, 01187 Dresden, Germany*
[4]*Centro Atómico Bariloche, Comisión Nacional de Energía Atómica, Consejo Nacional de Investigaciones Científicas y Técnicas,*
R8402AGP San Carlos de Bariloche, Río Negro, Argentina
[5]*Department of Physics, Clarendon Laboratory, University of Oxford, Park Road, Oxford OX1 3PU, United Kingdom*
[6]*Max Planck Institute for the Physics of Complex Systems, 01187 Dresden, Germany*
[7]*School of Physics and Astronomy, University of St Andrews, KY16 9SS St Andrews, United Kingdom*

Metamagnetic transitions are analogs of a pressure-driven gas-liquid transition in water. In insulators, they are marked by a superlinear increase in the magnetization that occurs at a field strength set by the spin exchange interactions. Here we study *topological* metamagnets, in which the magnetization is itself a topological quantity and for which we find a *single* transition line for two materials with substantially different magnetic interactions: the spin ices $Dy_2Ti_2O_7$ and $Ho_2Ti_2O_7$. We study single crystals under magnetic field and stress applied along the [001] direction and show that this transition, of the Kasteleyn type, has a magnetization versus field curve with upward convexity and a distinctive asymmetric peak in the susceptibility. We also show that the dynamical response of $Ho_2Ti_2O_7$ is sensitive to changes in the Ho^{3+} environment induced by compression along [001]. Uniaxial compression may open up experimental access to equilibrium properties of spin ice at lower temperatures.

I. INTRODUCTION

A. Motivation

Metamagnetism is the sudden increase in the magnetization of a material M induced by a small increase in magnetic field B. As in the liquid-gas transition, to which it is analogous, there is no spontaneous symmetry breaking involved. Metamagnets can be split into two main branches: metals and insulators. Here we concentrate on the latter, whose energy scale for metamagnetism is conventionally directly related to magnetic exchange interactions.

Among the magnetic insulators, topological spin liquids—systems that remain disordered but strongly correlated down to the lowest temperatures [1,2]—seem like unlikely places for metamagnetism to be found. We argue that this is not the case by considering two different instances of metamagnetic transitions in *spin ice*, a classical spin liquid characterized by an emergent gauge field and fractionalized excitations [3,4]. The first instance dates back to an experiment in 2003 [5]: a magnetic field applied along the [111] crystal direction was seen to destroy the dipolar spin correlations that betray the

presence of an emergent gauge field [4,6–8] while inducing a sudden increase in magnetization. The measured metamagnetic field is proportional to the effective exchange interaction imposing the spin correlations and is thus significantly different in the two canonical spin-ice materials: $Dy_2Ti_2O_7$ and $Ho_2Ti_2O_7$ [5,9]. In further analogy to the water-vapor transition, the phase diagram consists of a first-order line ending at a critical point [3,5].

The identification of a second type of metamagnetic behavior in these disordered materials, "topological metamagnetism," is the main finding of this paper. It involves a sweep through different topological sectors of the gauge field, as the magnetization corresponds to an average emergent gauge flux density. The location of this phenomenon, related to a three-dimensional Kasteleyn transition proposed more than a decade ago [10], does not depend on the value of exchange interactions. The system remains within the original ground state manifold, with the entropy associated with linelike excitations (and not the exchange interaction) competing with the Zeeman energy [10,11]. As a consequence, we will see that $Dy_2Ti_2O_7$ and $Ho_2Ti_2O_7$, with similar magnetic moments, share a single phase diagram. As in other metamagnetic transitions, there is no symmetry breaking between the saturated and unsaturated phases. However, as these phases belong to different topological sectors, the connectivity and other details of the phase diagram are different from those in conventional metamagnets. Finding macroscopic evidence for spin liquids

*Present address: European Molecular Biology Laboratory, 69117 Heidelberg, Germany.
†sag@iflysib.unlp.edu.ar
‡borzi@fisica.unlp.edu.ar

is notoriously difficult [1,2,12]; the realization of topological metamagnetism provides a direct link to the underlying gauge field in these materials.

B. Background

Dy$_2$Ti$_2$O$_7$ (DTO) and Ho$_2$Ti$_2$O$_7$ (HTO) are the most widely studied spin-ice materials [13]. Their rare-earth magnetic moments form a pyrochlore lattice of Ising *spins* [see inset in Fig. 2(a)] which can point only toward or away from the centers of the tetrahedral plaquettes [14]. The effective nearest-neighbor interaction, composed of exchange and dipolar terms, is ferromagnetic, with $J_{\mathrm{eff}} \approx 1.1$ K for DTO and ≈ 1.8 K for HTO. This is the sole energy scale of the nearest-neighbor (NN) model, which has ground state configurations with two spins pointing in and two out for any tetrahedron [empty tetrahedra in Fig. 2(a)]. This local rule allows for the magnetization to be interpreted as a divergence-free gauge field. The breaking of the spin balance in a tetrahedron, with three in/one out or one in/three out configurations, is thus seen as a local excitation or *monopole* [15] [colored spheres in Fig. 2(a)], which is crucial to understanding the materials' dynamics and thermodynamics [3,14,16,17]. The strong long-range dipolar interactions between spins (the magnetic moments in DTO and HTO are $\approx 10\mu_B$) can be approximately taken into account by two terms: the energy needed to create monopoles from the spin-ice manifold and a *magnetic Coulomb interaction* between them. This is the basis of the "dumbbell model" [3].

At low temperatures, a magnetic field **B**$||[001]$ polarizes all spins, selecting a single saturated configuration from the vast spin-ice manifold. If $T \ll J_{\mathrm{eff}}$, the density of monopoles ρ is exponentially small at any field. It follows that on decreasing B, the only mechanism that decreases M and increases the entropy is the introduction of extended excitations in the form of strings of reversed spins spanning the crystal [red arrows in Fig. 2(a)]. Topologically, this is not dissimilar to the entry of field lines in a type II superconductor. The transition here is of Kasteleyn type [18,19], and unlike in the previous two-dimensional case [7,20,21], it now takes place in three dimensions [10]. Crucially, the topological nature of the magnetization gives rise to an asymmetric susceptibility: it diverges below the critical field B_K and exactly vanishes above it [10], with $B_K/T = \mathrm{const}$ for the NN model [22]. At nonzero temperature, the presence of magnetic monopoles allows for shorter, nonspanning strings, which round the transition and dilute metamagneticlike features [10,11,16]. Experimentally, diffuse neutron scattering measurements in DTO crystals with field along [001] showed the existence of stringlike excitations and the ability of the magnetic field to orient them [16]. Magnetization measurements were used in this experiment to identify a dynamically active region in the T-B plane where equilibrium properties could be measured by neutron diffraction, and an approximate phase diagram, with frozen, "liquid," and saturated regions, was constructed. The boundary between the liquid and saturated regions is related to the Kasteleyn transition. Our experimental data now show evidence of a different type of *metamagnetic* behavior in connection with the transition, which we demonstrate is a direct consequence of the topological constraints imposed
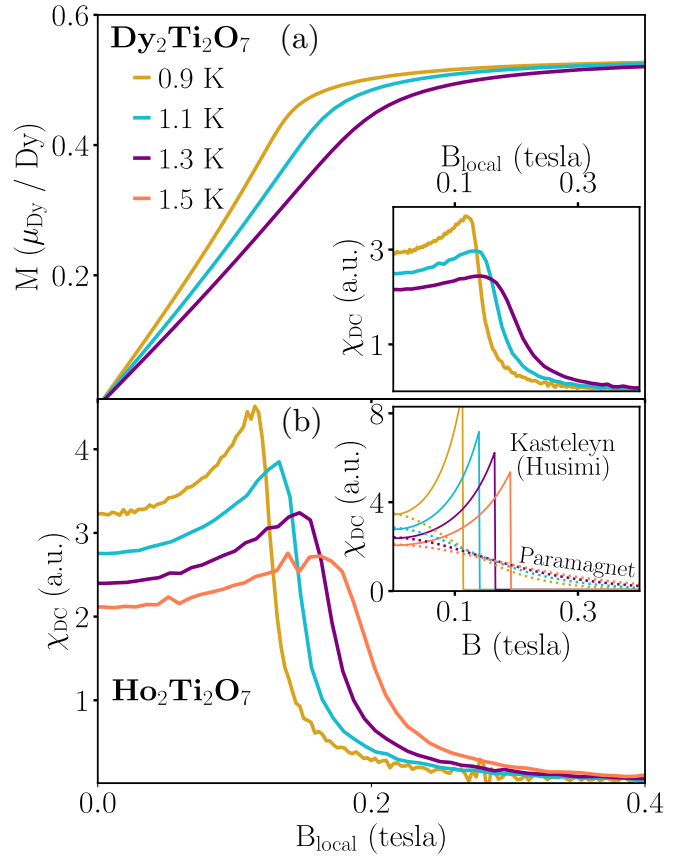

FIG. 1. (a) Magnetization M and static susceptibility ($\chi_{\mathrm{DC}} \equiv dM/dB_{\mathrm{local}}$, inset) for DTO as a function of internal magnetic field along [001] B_{local} at different temperatures. (b) χ_{DC} for HTO as a function of internal magnetic field. The metamagneticlike features are sharper for HTO than DTO, in agreement with its smaller density of local excitations (monopoles) at a given temperature. Inset: Ideal paramagnetic behavior (dotted lines) and Husimi tree results for the NN model without monopole excitations. The shape and behavior of the χ_{DC} peaks support a Kasteleyn transition broadened by thermal effects.

by the emergent gauge field. The static data and also the dynamic data—affected by the presence of extended excitations near the Kasteleyn transition—converge into a single experimental phase transition curve. Stressing that the underlying phenomenon is a topological change in their common ground state manifold, the phase diagrams coincide, within experimental error, for DTO and HTO, in spite of the differences between these materials. Adding to this, we study the thermodynamic and magnetic dynamics changes under strain.

II. RESULTS

We begin by analyzing the unstrained samples. The isothermal magnetization M for both compounds was studied at temperatures above the dynamical freezing regimes ($T > 0.7$ K) [23–27]. Figure 1(a) shows $M(T, B_{\mathrm{local}})$ along the [001] crystalline axis of a DTO single crystal as a function of local field B_{local}, obtained after correcting for demagnetization effects (see the Appendix). In the limit of high B_{local} the magnetization tends to saturate near $0.577\mu_{Dy}$/Dy, the
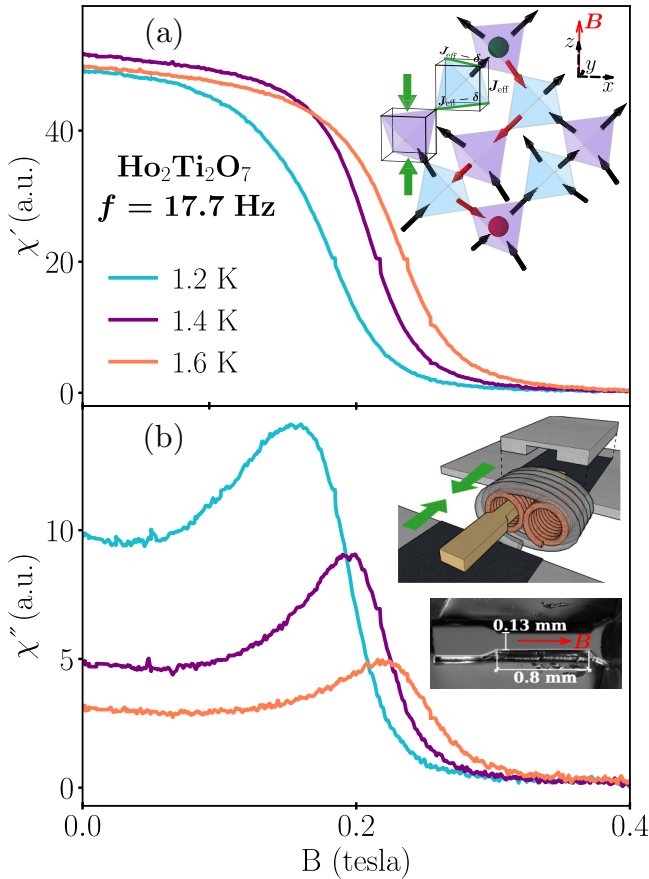
FIG. 2. (a) Real (χ') and (b) imaginary (χ'') parts of the ac susceptibility in unstrained HTO as a function of **B**||[001] for different temperatures. The monotonic $\chi'(B)$ contrasts with the peaks in χ'' at fields near those observed in χ_{DC}. The inset in (a) shows the pyrochlore spin lattice. A strong **B**||[001] polarizes all spins (black arrows); in red, a string of reversed spins is excited at a finite temperature. Tetrahedra with two spins in and two out are magnetically neutral; an imbalance of spins results in a positive or negative magnetic monopole (blue and red spheres). The green arrows mark the direction of compression. The insets in (b) show the HTO crystal, cut in an hourglass shape along [001] (bottom), and the susceptometer and strain device (top). The superconducting primary (gray) winds around the two mutually opposing secondary coils (orange). The ends of the sample were epoxied to mobile piezoelectric anvils and covered by metallic plates.

theoretical value [28]. The magnetization of an ideal paramagnet increases as a downward convex function for all fields; instead, the magnetization curve of DTO resembles that of a metamagnet, with an *upward* convexity over a broad range of intermediate B_{local}. This is more clearly seen in the derivative $dM/dB_{local} \equiv \chi_{DC}$, the static susceptibility (see the inset). The evolution of χ_{DC} at low fields and high T suggests a single characteristic energy scaling with B. However, rather than the monotonically decreasing χ_{DC} of paramagnets [inset in Fig. 1(b)], in DTO the susceptibility *increases* with field and vanishes after it peaks. As the temperature is lowered, the peak narrows and becomes more asymmetric. Sharper peaks, with the same characteristic asymmetry and at matching values of B_{local}/T, are seen in HTO [Fig. 1(b)]. It is helpful to compare

this transition to the known metamagnetic transition in spin ice at low T and B||[111] [5]. This sharp increase in M is observed for both canonical spin-ice materials at very different magnetic fields, proportional to their respective J_{eff} [5,9]. In contrast, the coincidence in B_{local}/T we now observe for the susceptibility peak maximum for **B**||[001] is already a strong indication that this feature does not correspond to standard metamagnetism.

The asymmetric nature of the peaks in χ_{DC} is another indication. The Kasteleyn transition is, indeed, characterized by such marked asymmetry since string excitations exist on only one side of the transition. This is clearly seen in the inset in Fig. 1(b), which shows a Husimi tree calculation of χ_{DC} for the NN model without monopolar excitations ($T \ll J_{eff}$) [29]. In our experiments the temperature is comparable to J_{eff}, and χ_{DC} is rounded off by finite-size string excitations that exist on both sides of the transition (not unlike the effect of finite size [22]); nonetheless, the curves retain the main signatures of a Kasteleyn transition. Indeed, the higher value of J_{eff}/T for HTO explains why narrower, taller, and more asymmetric peaks are observed in this material [30].

In order to analyze the in-field dynamics and to study the system under uniaxial pressure, we performed ac susceptibility measurements. Usually, a measurement at low frequencies ($\approx$10 Hz) would give a real part of the susceptibility χ' almost identical to the static χ_{DC} and a small imaginary part χ'' [24]. That is not the case here, even at the lowest frequencies we measured ($\approx$1 Hz). Figure 2(a) shows $\chi'(B)$ at 17.7 Hz, measured for a single crystal of HTO; within the temperature range inspected and for both compounds, we observed no peak in these curves. Remarkably, a peak instead appears in $\chi''(B)$ [see Fig. 2(b)], at fields near those found in χ_{DC}. At a given T the field position of the peak increases slightly with decreasing frequency (see the Appendix). The trend is more marked for DTO (with slower dynamics at these temperatures) and increases with decreasing T. This reflects the dynamical nature of the peak in χ''.

A common factor in both χ_{DC} and χ'' for both materials is to have a peak near $B/T \approx 0.1$ T/K. This can be used to separate two regions in the field-temperature plane: a low-field, high-temperature region where extended fluctuations that lower the magnetization proliferate and a high-field, low-temperature one where fluctuations are scarce and the magnetization is close to saturation. Figure 3 shows a collection of data points associated with these maxima for both materials. The data are representative of different samples, techniques, and instruments, with characteristic measurement times chosen to reflect information near the static limit. At low temperatures, the χ'' points collected for HTO were obtained with our bespoke susceptometer at zero strain, after linear extrapolation of the field maximum in χ'' to the limit $f \to 0$ (see the Appendix); those for DTO were measured at $f = 1.7$ Hz. The faster dynamics of HTO at higher temperatures allowed us to use data obtained at 77 Hz (with a bigger signal and less data treatment).

The data enable the construction of a curve that is, within error, independent of the material and technique used (Fig. 3). This independence allows us to associate this line of maxima with metamagnetism linked to topological changes in the emergent gauge field and the phase diagram with that of the
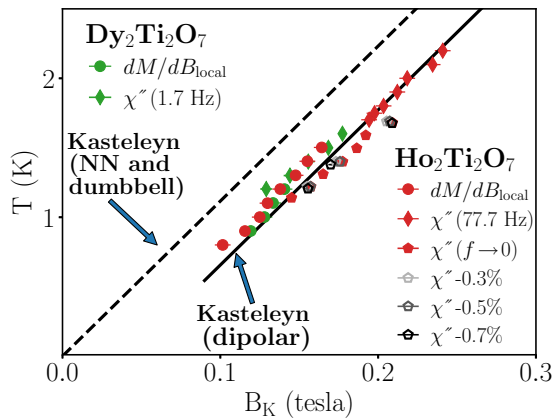
FIG. 3. The experimental points, obtained for materials with different J_{eff} and diverse measurement techniques, determine a single line that separates two regions: a high B/T region where the magnetization is close to saturation and a low one where fluctuations proliferate. The coincidence (within experimental error) of theses curves for HTO and DTO reflects the topological nature of the transition. The lines indicate the Kasteleyn transition curve for the NN and dumbbell models (dashed line, taken from Ref. [10]) and extrapolated from high T for the dipolar model (solid line, taken from Ref. [22]). The open pentagons are the results for χ'' ($f \rightarrow 0$) under strain.

three-dimensional Kasteleyn transition for spin as if $T \ll J_{eff}$ [10,11]. The dashed line indicates the predicted transition curve for a nearest-neighbor model [10]. The solid line corresponds to this curve corrected by dipolar interactions [22]: it is a much better match to the experimental points.

The dumbbell approximation has successfully explained several dynamical [14,17,27,31,32] and thermodynamical facts [3,14,16,32,33]. Since the Kasteleyn transition takes place in the limit of no monopolar excitations, in the absence of demagnetization effects it should be identical in both the NN and dumbbell models. In the latter, metamagnetism should be interpreted as a transition of the monopole vacuum. Corrections to this idealized model, similar for both materials, seem to account for the differences from the experimental results [34]. We find this remarkable since thermodynamic data at low fields are expected to differ from the dumbbell model only when T is of the order of a few hundred millikelvin [22,35–38].

The influence of the dipolar interaction on the peak position might, at first sight, seem to be at odds with the independence of the topological metamagnet from the strength of the effective interactions J_{eff}. That is not the case. The nearest-neighbor term of the dipolar interactions is, indeed, the major contribution to J_{eff} and is responsible for enforcing the emergence of the gauge field. An increase in this nearest-neighbor term, however big, would not change the low-temperature properties of the Coulomb phase; instead, it would increase only the temperature at which the topological effects are observed. The long-range part of the dipolar interactions is captured by the dumbbell model [3,6], but corrections are needed in the intermediate range. At a mean field level their effect is to reduce the magnetic enthalpy for

the creation of strings in the fully polarized phase, and thus, it shifts the topological transition along the field axis [22,38].

The change in the dynamic regime marked by the maximum in $\chi''(T, B)$ is rooted in several facts. The depletion of magnetic charges is particularly important for **B**||[001] and is quite abrupt near the transition [27]. This lowers the spin-flip rate at low temperatures and reduces the screening [14]. Additionally, by polarizing the magnetic moments, the static magnetic field changes the background in which the magnetic monopoles move. All this slows down the magnetic response of the system to an external field, reducing the blocking temperature [27]. The peak in χ_{DC} observed in Fig. 1 on decreasing field at low temperatures reflects the abrupt creation and/or marked development of long strings of inverted spins, driven by entropic forces. The absence of a peak in $\chi'(T, B)$ reflects the inability of these extended objects to oscillate in phase with the field even at frequencies as low as 1 Hz; they are instead seen in $\chi''(T, B)$. Dynamics is thus also markedly affected near the transition by the underlying topological changes in the gauge field.

Our bespoke ac susceptibility setup allows us to apply compressive uniaxial stress along the field direction [insets in Fig. 2(b)]. Theoretical work [39] predicts that B_K should decrease for crystals under compression along [001], through the progressive imbalance of exchange interactions [inset in Fig. 2(a)]. A recent study on HTO [40] reported a small evolution of J_{eff} with uniaxial pressure. Accordingly, the changes we observe in the position of the transition are almost negligible for the compression strengths that were experimentally accessible to us. This is seen in Fig. 3, where the open pentagons correspond to the $\chi''(B)$ peaks, after taking the $f \rightarrow 0$ limit, for different induced strain values.

However, the effect of an applied stress on a crystal can go beyond thermodynamics. Altering the environment of a spin may enhance quantum tunneling between its two Ising states and thus change its dynamical response [41–43]. It was theoretically proposed for $Tb_2Ti_2O_7$, an Ising pyrochlore with physics less understood than spin ice [44], that a tetragonal distortion can lead to faster dynamics [43]; this, together with the susceptibility of the non-Kramers HTO ground state doublet to transverse fields [42], might give the dynamics of HTO a high sensitivity to uniaxial pressure. Figure 4 shows χ''_{AC} at $f = 1117.7$ Hz and $B = 0$ as a function of temperature for different compressive strains. As seen there, the position of the peak is sensitive to the applied stress and moves markedly toward lower temperatures: at a given T the response times shorten as the environment is distorted. The temperature at which a relaxation time of the order of 1 ms is reached is decreased by more than 0.15 K for -0.6% distortion. We believe that this observation, combined with the lack of a measurable effect in the thermodynamic properties, may open an interesting avenue of research. Uniaxial stress in a material like HTO with a small exchange constant (dominated by the NN term in the dipolar interactions) could be a route toward a canonical spin ice with faster dynamics. If the effect were to continue to lower temperatures, it might open the possibility of experimentally detecting signs of the long-sought ordered ground state [35,38,45–48]. Similarly, the ability to alter the environment of these *a priori classical* spins could constitute a route toward inducing tunable quantum effects. Our first
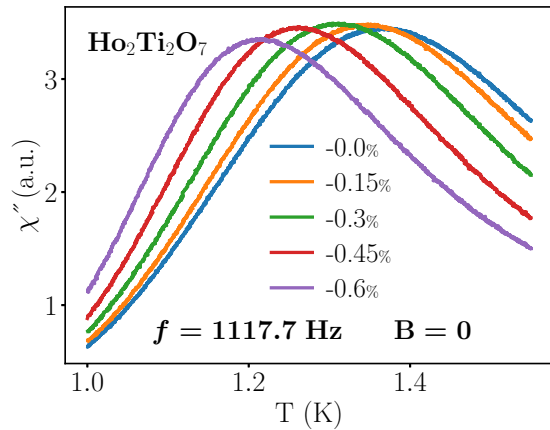
FIG. 4. Imaginary part of the ac susceptibility χ'' for HTO at zero field, measured as a function of temperature at fixed frequency f for different values of strain along [001]. The peak moves toward lower temperatures as compression increases, indicating a faster dynamics.

results for strain-induced manipulation of the dynamics indicate clear promise for further work in this direction.

III. DISCUSSION

Experimental studies on the magnetization process under the applied field of two different spin-ice materials along the [100] crystal direction led us to identify what may be called *topological metamagnetism*, in which the nonanalytical behavior of the magnetization is driven by the topological nature of the underlying gauge field. It is thus remarkable that topological effects are evident in macroscopic measurements, shaping the magnetization curves and affecting its dynamics. We find that M increases with field with *upward* convexity, a reflection of the flattening of the entropy as a function of magnetization near zero entropy, in turn linked to the presence of string defects in the otherwise polarized gauge field [10,11].

Combining magnetization and ac susceptibility measurements and taking advantage of the unusual dynamics of this transition arising from the spatially extended nature of the excitations, we constructed a detailed phase diagram of its associated three-dimensional Kasteleyn transition and compared it with theoretical predictions. The experiments show that dipolar interactions need to be taken fully into account to successfully model the Kasteleyn transition line. The nature of the dipolar term (which is only approximately taken into account by the dumbbell model at intermediate ranges) affects the otherwise flat energy landscape of the ground state manifold [49] and thus the energetics of the gauge field. It then shifts the transition line toward higher fields and lower temperatures. In spite of the different magnetic interactions J_{eff} naturally leading to different transitions fields for the metamagnetism along [111], we obtain a single phase diagram for both compounds with field along [001]. This can be explained by the fact that (independent of the magnitude of J_{eff}) both materials share a ground state manifold, which is described by the same gauge field. Furthermore, due to the similarity of the dipolar magnetic moments associated with Dy^{3+} and Ho^{3+}, dipolar corrections beyond the dumbbell model are also expected to be similar in both cases. Further corrections

due to effective exchange interactions for second and third neighbors, known to be present in DTO [45,46,48,50] and HTO [45], would also affect the phase diagram; our present results suggest they are not of much significance here.

Uniaxial stress applied to $Ho_2Ti_2O_7$ leads to faster dynamics at ≈ 1 kHz, with canonical spin-ice thermodynamic behavior. It is thus tempting to conjecture that this might open the possibility to study these materials in an as yet unexplored regime by lowering the dynamical freezing temperature. By the same token, applied stress also opens the possibility to modify the environment of the magnetic ion and might lead to quantum effects in these hitherto completely "classical" spin-ice materials. Further studies are necessary to determine the dependence of the magnetic relaxation time on deformation and temperature to establish whether the observed trend continues at higher stress and lower frequencies and also to see whether there is a direction of compression (or tension) that optimizes the dynamical effects without compromising the thermodynamics and whether high enough compression/tension can be attained.

APPENDIX: MATERIALS AND METHODS

1. Samples

The DTO and HTO samples used in this paper were grown in St Andrews and Oxford using floating zone furnaces. For the strain measurements we used a HTO single crystal, with the approximate dimensions 1.9×0.34 mm^2 and a thickness of 0.13 mm, cut along its principal axes. It was then etched using a Xenon Plasma Focused Ion Beam into an hourglass shape (see insets in Fig. 2 in the main text). This shape allowed us to achieve high homogeneous compression in the middle section of the sample where the actual measurement took place. The samples used for the other measurements were two single crystals of $Ho_2Ti_2O_7$ and $Dy_2Ti_2O_7$, with approximate dimensions $2.8 \times 0.75 \times 0.55$ mm^3 and $4.55 \times 0.71 \times 0.66$ mm^3, respectively. In all samples, the susceptibility was measured with the longer side of the sample along the magnetic field direction in order to minimize demagnetization effects.

2. Measurements

The experiments were performed at two different locations, with several instruments and different samples. The magnetization measurements were carried out using a commercial Quantum Design magnetic property measurement system (MPMS). The standard field sweep rate used was
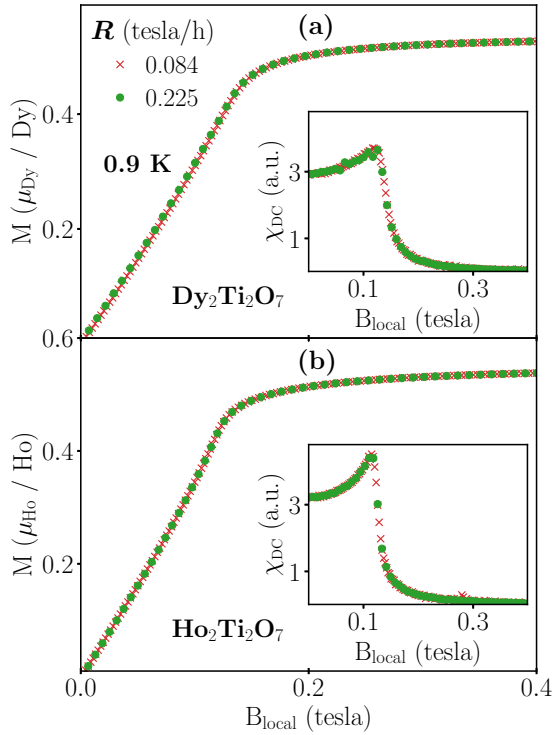
FIG. 5. Magnetization M and static susceptibility χ_{DC} (inset) at 0.9 K for (a) DTO and (b) HTO as a function of internal magnetic field along [001] B_{local}. We have used two field sweep rates $R \equiv dB/dt$ differing by a factor of ≈ 3, obtaining the same results. This suggests that the measurements approach the static limit. It is easy to see that the superlinear increase in the magnetization indicating metamagnetism (correlated to a susceptibility peak) is much better defined and more asymmetric for HTO, where the spin-ice condition two spins in/two out at a given temperature is fulfilled for a much bigger fraction of tetrahedra. The positions of the susceptibility peak are very similar in both cases, in spite of the marked differences in their effective nearest-neighbor magnetic interactions J_{eff}.

$R \equiv dB/dt = 0.225$ T/h. In order to check that these measurements were a good approximation to the static limit, we repeated the curves at low temperature (here 0.9 K) at two different field sweep rates for both compounds. Figure 5 shows the magnetization and $\chi_{DC} \equiv dM/dB_{local}$ for DTO [Fig. 5(a)] and HTO [Fig. 5(b)]. There is no evident field rate dependence in any of the compounds despite R varying by a factor of almost 3.

We used three different probes for the ac susceptibility measurements. The first part of the measurements was carried out with a bespoke probe in a single-shot ^{3}He cryostat. The susceptometer consisted of a pair of counterwound pickup coils, each with approximately 1200 turns of a 60 μm diameter copper wire. In order to guarantee good thermal contact the probe was immersed in the He^3 chamber. The ac field used was 1.75×10^{-4} T. The second part was performed in a commercial Quantum Design physical property measurement system. Finally, the susceptibility under applied strain (including zero compression) was measured in a dilution refrigerator; in order to work at temperatures above 1.1 K, the normal regime of operation was changed by partially decoupling the probe from the mixing chamber.
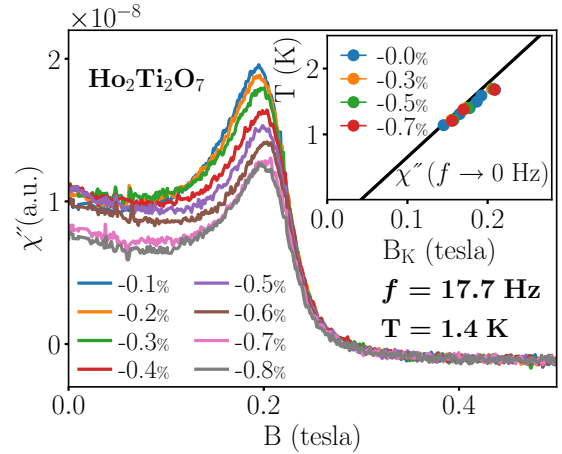

FIG. 6. Effects of compression. Imaginary part of the susceptibility χ''_{AC} vs field along [001] for different values of applied stress parallel to **B**. In all cases the temperature is fixed at 1.4 K, and the frequency is fixed at $f = 17.7$ Hz. The inset shows the phase diagram under compressing strain for $f \rightarrow 0$. The solid line indicates the predicted Kasteleyn transition in the presence of dipolar interactions under no applied stress.

In this case, the extremely delicate pickup coils consisted of two counterwound secondary coils (≈ 200 turns each) of an 11 μm diameter copper wire; the primary coil was wound around them with 20 turns of 60 μm superconducting wire [see Fig. 2(b) in the main text]. The excitation ac field used was $\approx 8 \times 10^{-4}$ T.

The strain was applied using a piezoelectric-based uniaxial pressure cell with integrated force and displacement sensors developed at the Max Planck Institute for Chemical Physics of Solids in Dresden, Germany [51,52].
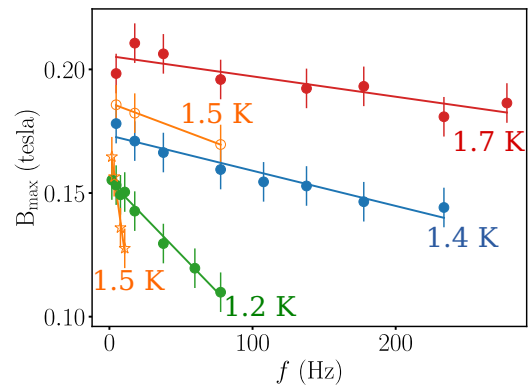

FIG. 7. Extrapolation to $f \rightarrow 0$. Each point represents the field maximum B_{max} in the imaginary part of the ac susceptibility $\chi''(T, B)$ at a given temperature T and frequency f. Solid circles: Ho$_2$Ti$_2$O$_7$ crystals at a fixed strain of -0.3%. B_{max} increases with decreasing frequency, a trend that is more pronounced at low temperature. The points in the phase diagram corresponding to $f \rightarrow 0$ were taken after a linear extrapolation, as illustrated here. Open symbols: Ho$_2$Ti$_2$O$_7$ (circles) and Dy$_2$Ti$_2$O$_7$ crystals (stars) at nominally zero compression. The curves have a bigger negative slope for DTO at fixed temperature, reflecting its slower dynamics in our working temperature range.

3. Local versus applied field

The magnetic field B was corrected by taking into account the demagnetizing factor D in order to obtain the internal magnetic field B_{local} at the peak of the static or dynamic susceptibility. D was estimated with standard methods, assuming the samples were perfect rectangular prisms [53]. In the case of ac susceptibility, the magnetization at the peak of its imaginary part was taken from the MPMS measurements. We also estimated B_{local} with the aid of Monte Carlo simulations; the difference between these procedures was used as a way to estimate the error in the peak location. Due to the sample shape, the magnitude of the distortions, and the smallness of the demagnetization factor, we did not consider changes in D when straining the crystals.

4. Imaginary part of the susceptibility under compression and extrapolation to $f \to 0$

Figure 6 shows χ'' for HTO as a function of $\mathbf{B}||[001]$ and $T = 1.4$ K; different values of strain were induced along [001], between -0.1% and -0.8% (the minus sign here indicates compression). At fixed $f = 17.7$ Hz the effect of compression is very modest: it slightly *increases* the field of the peak maximum. However, as explained below, when extrapolating the data to $f \to 0$, this tendency is almost canceled, indicating that the main effect of the uniaxial compressive stress is to accelerate the dynamics.

As mentioned in the main text, the peak at the field $B_{\max}$ observed in the imaginary part of the susceptibility χ'' not only depends on T but also shows a smooth dependence on the frequency f. As illustrated in Fig. 7, this dependence is stronger at lower temperatures (i.e., greater relaxation times) and very small at high temperatures. One way of approaching the three-dimensional Kasteleyn transition phase diagram is through the slow dynamics related to the creation or growth of sample-spanning strings of inverted spins. In the main text we observed that the peak in χ'' in the low-frequency limit coincides with the phase transition peaks observed for both DTO and HTO in static measurements. Figure 7 illustrates how the limit $f \to 0$ was taken.

[1] L. Balents, Nature (London) **464**, 199 (2010).

[2] J. Knolle and R. Moessner, Annu. Rev. Condens. Matter Phys. **10**, 451 (2019).

[3] C. Castelnovo, R. Moessner, and S. L. Sondhi, Nature (London) **451**, 42 (2008).

[4] C. L. Henley, Annu. Rev. Condens. Matter Phys. **1**, 179 (2010).

[5] T. Sakakibara, T. Tayama, Z. Hiroi, K. Matsuhira, and S. Takagi, Phys. Rev. Lett. **90**, 207205 (2003).

[6] S. V. Isakov, K. Gregor, R. Moessner, and S. L. Sondhi, Phys. Rev. Lett. **93**, 167204 (2004).

[7] T. Fennell, S. Bramwell, D. McMorrow, P. Manuel, and A. Wildes, Nat. Phys. **3**, 566 (2007).

[8] T. Fennell, P. Deen, A. Wildes, K. Schmalzl, D. Prabhakaran, A. Boothroyd, R. Aldus, D. McMorrow, and S. Bramwell, Science **326**, 415 (2009).

[9] C. Krey, S. Legl, S. R. Dunsiger, M. Meven, J. S. Gardner, J. M. Roper, and C. Pfleiderer, Phys. Rev. Lett. **108**, 257204 (2012).

[10] L. D. C. Jaubert, J. T. Chalker, P. C. W. Holdsworth, and R. Moessner, Phys. Rev. Lett. **100**, 067207 (2008).

[11] L. D. Jaubert, J. Chalker, P. Holdsworth, and R. Moessner, J. Phys.: Conf. Ser. **145**, 012024 (2009).

[12] L. D. C. Jaubert, M. J. Harris, T. Fennell, R. G. Melko, S. T. Bramwell, and P. C. W. Holdsworth, Phys. Rev. X **3**, 011014 (2013).

[13] S. T. Bramwell and M. J. Gingras, Science **294**, 1495 (2001).

[14] S. T. Bramwell and M. J. Harris, J. Phys.: Condens. Matter **32**, 374010 (2020).

[15] "All-in" and "all-out" excitations are also possible, but they are so energetically costly that they need not be considered here.

[16] D. J. P. Morris, D. A. Tennant, S. A. Grigera, B. Klemke, C. Castelnovo, R. Moessner, C. Czternasty, M. Meissner, K. C. Rule, J.-U. Hoffmann, K. Kiefer, S. Gerischer, D. Slobinsky, and R. S. Perry, Science **326**, 411 (2009).

[17] L. D. Jaubert and P. C. Holdsworth, Nat. Phys. **5**, 258 (2009).

[18] P. W. Kasteleyn, J. Math. Phys. **4**, 287 (1963).

[19] J. Nagle, Proc. Natl. Acad. Sci. U.S.A. **70**, 3443 (1973).

[20] R. Moessner and S. L. Sondhi, Phys. Rev. B **68**, 064411 (2003).

[21] A. A. Turrini, A. Harman-Clarke, G. Haeseler, T. Fennell, I. G. Wood, P. Henelius, S. T. Bramwell, and P. C. W. Holdsworth, Phys. Rev. B **105**, 094403 (2022).

[22] M. L. Baez and R. A. Borzi, J. Phys.: Condens. Matter **29**, 055806 (2017).

[23] K. Matsuhira, Y. Hinatsu, K. Tenya, and T. Sakakibara, J. Phys.: Condens. Matter **12**, L649 (2000).

[24] J. Snyder, B. G. Ueland, J. S. Slusky, H. Karunadasa, R. J. Cava, and P. Schiffer, Phys. Rev. B **69**, 064414 (2004).

[25] G. Ehlers, A. Cornelius, T. Fennell, M. Koza, S. Bramwell, and J. Gardner, J. Phys.: Condens. Matter **16**, S635 (2004).

[26] H. Takatsu, K. Goto, H. Otsuka, R. Higashinaka, K. Matsubayashi, Y. Uwatoko, and H. Kadowaki, J. Phys. Soc. Jpn. **82**, 104710 (2013).

[27] P. C. Guruciaga, L. Pili, S. Boyeras, D. Slobinsky, S. A. Grigera, and R. A. Borzi, J. Phys.: Condens. Matter **32**, 425804 (2020).

[28] H. Fukazawa, R. G. Melko, R. Higashinaka, Y. Maeno, and M. J. P. Gingras, Phys. Rev. B **65**, 054410 (2002).

[29] L. D. Jaubert, Ph.D. thesis, Ecole Normale Supérieure de Lyon, 2009.

[30] Simulations for the dipolar Hamiltonian at $T = 0.9$ and $B = 0$ give $\approx 2\%$ of tetrahedra occupied by monopoles for DTO: an order of magnitude larger than for HTO under the same conditions.

[31] S. Mostame, C. Castelnovo, R. Moessner, and S. L. Sondhi, Proc. Natl. Acad. Sci. U.S.A. **111**, 640 (2014).

[32] C. Castelnovo, R. Moessner, and S. L. Sondhi, Phys. Rev. B **84**, 144435 (2011).

[33] P. C. Guruciaga, S. A. Grigera, and R. A. Borzi, Phys. Rev. B **90**, 184423 (2014).

[34] We have not tried to include other perturbation terms, such as second- or third-NN interactions [45,46,48,50].

[35] R. G. Melko, B. C. den Hertog, and M. J. P. Gingras, Phys. Rev. Lett. **87**, 067203 (2001).

[36] D. Pomaranski, L. Yaraskavitch, S. Meng, K. Ross, H. Noad, H. Dabkowska, B. Gaulin, and J. Kycia, Nat. Phys. **9**, 353 (2013).

[37] R. A. Borzi, D. Slobinsky, and S. A. Grigera, Phys. Rev. Lett. **111**, 147204 (2013).

[38] S.-C. Lin and Y.-J. Kao, Phys. Rev. B **88**, 220402(R) (2013).

[39] L. D. C. Jaubert, J. T. Chalker, P. C. W. Holdsworth, and R. Moessner, Phys. Rev. Lett. **105**, 087201 (2010).

[40] R. Edberg, I. M. B. Bakke, H. Kondo, L. Ø. Sandberg, M. L. Haubro, M. Guthrie, A. T. Holmes, J. Engqvist, A. Wildes, K. Matsuhira, K. Lefmann, P. P. Deen, M. Mito, and P. Henelius, Phys. Rev. B **102**, 184408 (2020).

[41] B. Tomasello, C. Castelnovo, R. Moessner, and J. Quintanilla, Phys. Rev. B **92**, 155120 (2015).

[42] B. Tomasello, C. Castelnovo, R. Moessner, and J. Quintanilla, Phys. Rev. Lett. **123**, 067204 (2019).

[43] P. Bonville, I. Mirebeau, A. Gukasov, S. Petit, and J. Robert, Phys. Rev. B **84**, 184409 (2011).

[44] M. Enjalran, M. J. Gingras, Y. Kao, A. Del Maestro, and H. Molavian, J. Phys.: Condens. Matter **16**, S673 (2004).

[45] R. A. Borzi, F. A. Gómez Albarracín, H. D. Rosales, G. L. Rossini, A. Steppke, D. Prabhakaran, A. P. Mackenzie, D. C. Cabra, and S. A. Grigera, Nat. Commun. **7**, 12592 (2016).

[46] P. Henelius, T. Lin, M. Enjalran, Z. Hao, J. G. Rau, J. Altosaar, F. Flicker, T. Yavors'kii, and M. J. P. Gingras, Phys. Rev. B **93**, 024402 (2016).

[47] S. R. Giblin, M. Twengström, L. Bovo, M. Ruminy, M. Bartkowiak, P. Manuel, J. C. Andresen, D. Prabhakaran, G. Balakrishnan, E. Pomjakushina, C. Paulsen, E. Lhotel, L. Keller, M. Frontzek, S. C. Capelli, O. Zaharko, P. A. McClarty, S. T. Bramwell, P. Henelius, and T. Fennell, Phys. Rev. Lett. **121**, 067202 (2018).

[48] A. M. Samarakoon, K. Barros, Y. W. Li, M. Eisenbach, Q. Zhang, F. Ye, V. Sharma, Z. L. Dun, H. Zhou, S. A. Grigera, C. D. Batista, and D. A. Tennant, Nat. Commun. **11**, 892 (2020).

[49] A. M. Samarakoon, A. Sokolowski, B. Klemke, R. Feyerherm, M. Meissner, R. A. Borzi, F. Ye, Q. Zhang, Z. Dun, H. Zhou, T. Egami, L. Jaubert, C. Castelnovo, R. Moessner, S. A. Grigera, and D. A. Tennant, arXiv:2107.12305.

[50] T. Yavors'kii, T. Fennell, M. J. P. Gingras, and S. T. Bramwell, Phys. Rev. Lett. **101**, 037204 (2008).

[51] C. W. Hicks, M. E. Barber, S. D. Edkins, D. O. Brodsky, and A. P. Mackenzie, Rev. Sci. Instrum. **85**, 065003 (2014).

[52] M. E. Barber, A. Steppke, A. P. Mackenzie, and C. W. Hicks, Rev. Sci. Instrum. **90**, 023904 (2019).

[53] A. Aharoni, J. Appl. Phys. **83**, 3432 (1998).